Acta Polytechnica **54**(4):266–270, 2014
doi:10.14311/AP.2014.54.0266

available online at http://ojs.cvut.cz/ojs/index.php/ap

X-RAY VARIABILITY STUDY OF POLAR SCATTERED SEYFERT 1 GALAXIES

Tobias Beuchert[a,b,*], Jörn Wilms[a], Matthias Kadler[a,b], Anna Lia Longinotti[c], Matteo Guainazzi[c], Giovanni Miniutti[d], Ignacio de la Calle[c]

[a] *Dr. Karl Remeis-Observatory, Universität Erlangen-Nürnberg & ECAP, Sternwartstrasse 7, 96049 Bamberg, Germany*

[b] *Lehrstuhl für Astronomie, Universität Würzburg, Campus Hubland Nord, Emil-Fischer-Straße 31, 97074 Würzburg, Germany*

[c] *European Space Astronomy Centre of ESA, PO Box 78, Villanueva de la Cañada, 28691 Madrid, Spain*

[d] *Centro de Astrobiología (CSIC-INTA), Dep. de Astrofísica; ESAC, PO Box 78, E-28691 Villanueva de la Cañada, Madrid, Spain*

[*] corresponding author: tobias.beuchert@sternwarte.uni-erlangen.de

Abstract. We study 12 Seyfert 1 galaxies with a high level of optical polarization. Optical light emerging from the innermost regions is predominantly scattered in a polar region above the central engine directly in our line of sight. These sources show characteristics of Seyfert 2 galaxies, e.g. polarized broad lines. The polarization signatures suggest a viewing angle of 45°, classifying them as intermediate Seyfert 1/2 types. The unified model predicts this line of sight to pass through the outer layer of the torus resulting in significant soft X-ray variability due to a strongly varying column density. The aim is to find evidence for this geometrical assumption in the spectral variability of all available historical observations of these sources by *XMM-Newton* and *Swift*.

Keywords: variability, column density variation, unified model.

1. Introduction

According to the unified model of Active Galactic Nuclei/AGN [1] Seyfert 1 and Seyfert 2 galaxies are the same type of galaxies, but seen under different inclination angles (Fig. 1). At inclinations $\lesssim 45°$, Seyfert 1 galaxies are typically either optically unpolarized or polarized due to predominantly equatorial scattering. Seyfert 2 galaxies have an inclination of $\gtrsim 45°$ and show mainly optical polarization features due to polar-scattering, as the line of sight of Seyfert 2 galaxies passes through the optically thick torus. This picture usually works well, but [22] identify 12 Seyfert 1 galaxies that exhibit optical polarization similar to Seyfert 2 galaxies. They conclude that these polar-scattered Seyfert 1 galaxies are seen under an inclination of $i \sim 45°$ and thus represent the transition between unobscured Seyfert 1 and obscured Seyfert 2 galaxies (Fig. 1). The line of sight towards these galaxies therefore passes through the outer layers of the torus, where significant absorption is still expected and suppresses polarized light from the equatorial scattering region, but not the polar-scattered light. We assume these outer layers to be a non-homogeneous gas and dust medium which might be stripped off by nuclear radiation resulting in a highly variable column density towards the observer. X-ray observations of these polar-scattered Seyfert 1 galaxies should therefore exhibit a strongly variable N_{H}.

We compare the X-ray properties of a sample of 12 polar-scattered Seyfert 1 galaxies and 11 equatorial-scattered Seyfert 1 galaxies (see Table 1) for which no absorption variability is expected according to the line-of-sight. As of now, only the first set of polar-scattered Seyfert 1 galaxies has been analyzed. In Table 1, the dashed line separates sources with spectra of sufficient signal-to-noise to constrain the N_{H}(top) from sources with insufficient signal-to-noise (bottom). When studying the properties of absorption we have to take into account source intrinsic absorption of both neutral and ionized matter. The neutral, cold absorption can be due to spatially distinct regions in AGN. Theory [4, 9] predicts a relatively cold, dense phase in equilibrium with partially ionized gas forming the broad line region (BLR). These embedded BLR clouds are commonly believed to be gravitationally bound to the center of mass. They are good candidates to cause short occultation events with attenuated soft X-ray spectra. At larger distances to the central black hole, variable neutral structures can exist at the outer torus layer possibly evaporated due to the in-falling radiation [6]. Recent studies by [13] even demonstrate the relevance of a model where the torus consists of distinct clumps [14, 15]. Whereas cold absorbing gas and dust is still assumed to be confined to the obscuring torus, warm, partially ionized gas is often found to be outflowing [5]. MHD disk winds [7] are one theoretical explanation. Such so called warm

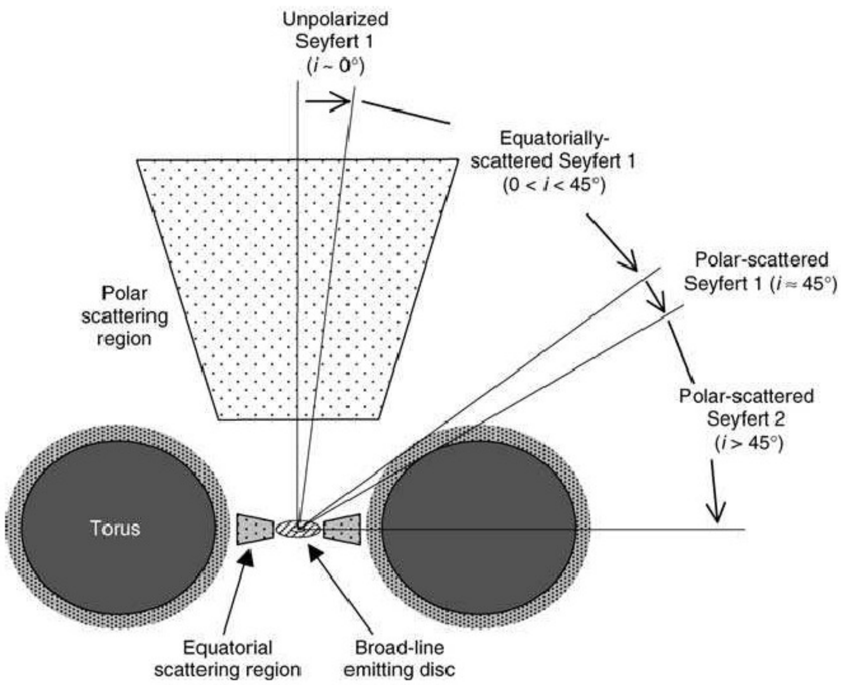

Figure 1. Polar and equatorial scattering regions according to the unified scheme of AGN. Adopted from [22].

Source name	*Swift* XRT	*XMM-Newton* pn
NGC 3227	7	2
NGC 4593	5	2
Mrk 704	5	2
Fairall 51	2	2
ESO 323-G077	3	1
Mrk 1218	7	2
UGC 7064	2	1
Mrk 766	33	15
Mrk 321	1	1
Mrk 376	2	
IRAS 15091−2107		1
Mrk 1239		1
Akn 120	3	1
1Zwl	7	2
KUV 18217+6419	1	22
Mrk 006	4	4
Mrk 304		2
Mrk 509	23	17
Mrk 841	4	5
Mrk 876	16	2
Mrk 985		
NGC 3783	6	4
NGC 4151	4	17

Table 1. The sample from Smith et al.: *top half:* polar-scattered Sy I galaxies, *bottom half:* equatorial scattered Sy I galaxies – the control sample. The numbers denote the amount of pointings with the corresponding satellite.

absorbers [19] can be separated from neutral absorbers with typical spectral features. In contrast to the dusty outer layer of the torus, we assume ionized absorbers to fully cover the line-of-sight [3].

2. Methods

Here we limit ourselves to the first sample of polar scattered Seyfert galaxies. The search for variability in these sources requires consistent model fitting in order to ensure that the detected variability of absorption indeed originates in the proposed region. An important task is to disentangle consistently the contributions of warm- and cold-absorption via spectral model fitting in order to locate the absorber. Distinguishing two absorption components, neutral and partially ionized, is a challenging task when dealing with low signal-to-noise spectra, such as *Swift* data. *XMM-Newton* observations, however, can help to constrain properties of one or more warm absorber phases. The picture becomes even more complicated when considering the warm absorber not to be a homogeneous gas but rather dynamic and indeed variable, both in covering fraction and column density as shown for Mrk 704 by [11]. As a consequence we cannot easily draw a conclusion on warm absorber parameters from one observation to another. As the partially ionized phase can also attenuate the soft continuum to some extent, we have to assume that both ionized and neutral phases do contribute to the overall continuum absorption within the suggested line-of-sight at $\sim 45°$ inclination.

Within this work, however, we are explicitly interested in the variability of neutral absorption. At

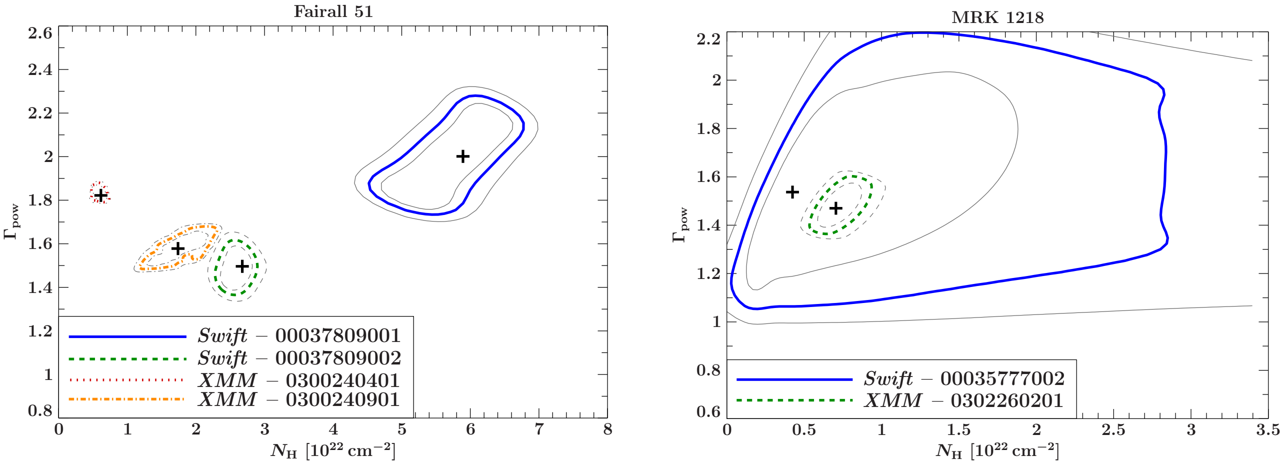

Figure 2. Combined contours of all observations of Fairall 51 (left) and Mrk 1218 (right) for 68.3 %, 90 % (blue) and 99 % confidence levels. The numbers within the plot panels are appropriate observation ids.

least for now we do not consider further the warm absorber contributions, unless explicitly necessary. When searching for variability, a consistency check of all modeled observations is necessary. This is done by examining correlations of column density related parameters of each fit and observation, and calculating appropriate confidence levels. In order to find appropriate model fits, a bottom-up procedure is chosen, starting with a power-law photon continuum,

$$N_{\mathrm{ph,full}}(E) = A_{\mathrm{full}} e^{-\sigma N_{\mathrm{H\,int}}} (E^{-\Gamma} + \mathcal{G}_{\mathtt{Fe}}) e^{-\sigma N_{\mathrm{H\,hal}}} \quad (1)$$

which is fully covered by Galactic and source-intrinsic neutral matter. We further test a model where the continuum source is partially covered by the source intrinsic absorber,

$$N_{\mathrm{ph,partial}}(E) = A_{\mathrm{partial}} \left[(1-c)\, c\, e^{-\sigma N_{\mathrm{H\,int}}}\right] \times (E^{-\Gamma} + \mathcal{G}_{\mathtt{Fe}}) e^{-\sigma N_{\mathrm{H\,gal}}} \quad (2)$$

and finally a partially covered source with an ionized medium in front of it (a “warm absorber”),

$$N_{\mathrm{ph,WA}}(E) = A_{\mathrm{WA}}\, \mathrm{WA}(1)\, \mathrm{WA}(2) \times e^{-\sigma N_{\mathrm{H\,int}}} (E^{-\Gamma} + \mathcal{G}_{\mathtt{Fe}}) e^{-\sigma N_{\mathrm{H\,gal}}}. \quad (3)$$

Which model is chosen depends on the signal to noise ratio of the data. Here the partial covering scenario is included in the warm absorber models. In addition to the continua above, the Fe Kα line at 6.4 keV is phenomenologically fitted with a Gaussian model component if existent. Compton reflection as a more physical model to explain features like the Fe Kα line is not included in the fits because of the lack of sensitivity above 10 keV, where Compton reflection dominates. Having found the best fitting model, the parameter space is further investigated to find the 90 % confidence levels for each parameter as well as confidence contours between correlated parameters. In particular, correlations between the neutral column density and the covering fraction as well as the power-law slope are of interest. Uncertainties of the column density are then derived from the 90 % confidence contours. The immediate aim is to search for significant variability of the measured column densities of a cold absorber that is assumed to be located in the outer torus layers and hence to underlie structural variability. The significance of variability is best evaluated by considering contours of all analyzed observations of one source (Fig. 2). The left panel of Fig. 2 shows that the column densities measured in different observations are inconsistent between different epochs, therefore implying a clear detection of variability in the case of Fairall 51. In contrast, in the case of Mrk 1218 (Fig. 2, right panel) the smaller contours of the *XMM-Newton* observation are fully enclosed by those of the *Swift* observation with less signal-to-noise. Both observations are consistent with each other and no variability can be claimed based on the given data. For models such as ours with several degrees of freedom as well as a limited number of bins, the typical parameter space is more or less asymmetric [2]. The results are asymmetric uncertainties. We derive combined column densities with unequal upper and lower uncertainties. Gaussian error propagation is not applicable in this case. A solution is given by [2] and is also applied in this work.

3. Results

We find 6 out of 12 sources of the sample to reveal variable absorption of the soft X-rays on timescales from days to years. For Mrk 766 as a well studied source [12, 23], minimum variability timescales on the basis of hours were found by [21]. Figure 3 shows an example of strong spectral variability in NGC 3227 with particularly changing warm absorption properties. Warm or (partially) gas still has a rich number of high-Z elements able to absorb soft X-ray photons. In addition to column density variations of such ionized gas, the ionization states are change between the *XMM-Newton* observations. These changes

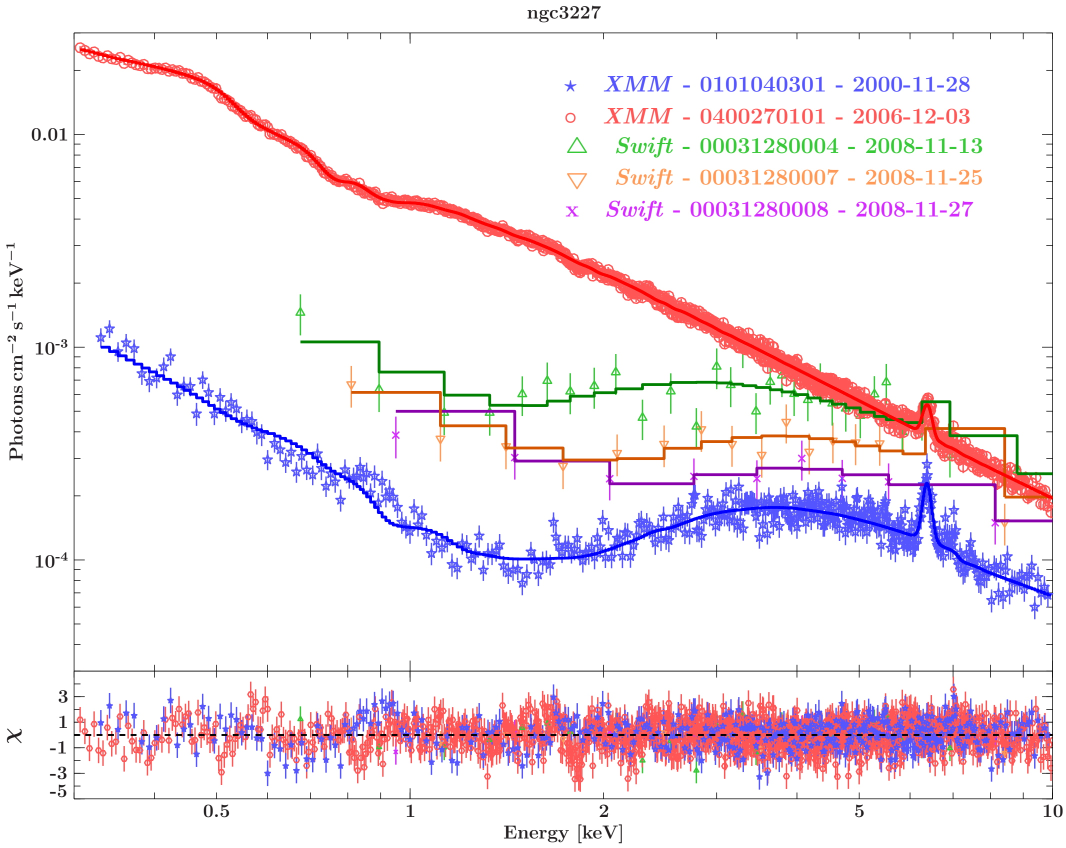

FIGURE 3. Spectral variability of NGC 3227.

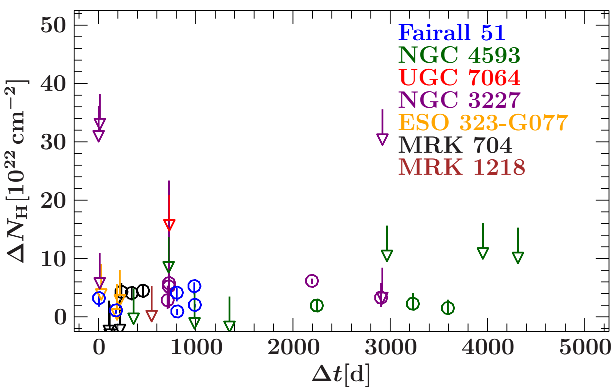

FIGURE 4. Plot of variability timescales measured between sub-sets of two observations against the corresponding difference in absorption for all sources with sufficient signal-to-noise ratios. All column densities are due to neutral matter except for Fairall 51, where only warm absorber phases can be constrained. The uncertainties are plotted at a 90 % confidence level.

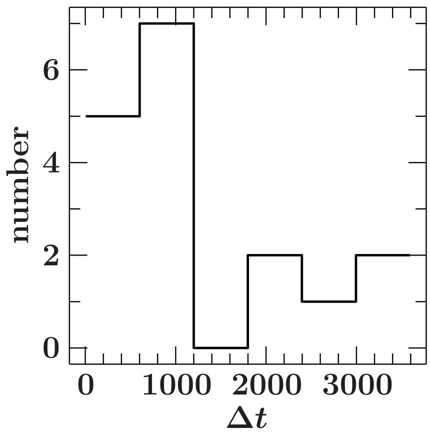

FIGURE 5. Distribution of all measured variability timescales in days.

are interpreted to be due to the varying irradiation expressed by a varying power-law norm. As the ionization parameter $\xi = L/N_{\rm H}r^2$ is proportional to the luminosity, it should behave directly proportional to it. This seems indeed to be the case for NGC 3227. Collecting the results from the analysis of the whole sample of polar-scattered Seyfert 1 galaxies, Fig. 4 shows the time differences between all possible pairs of observations of all sources against the appropriate column density differences throughout for all sources. For the cases where no $N_{\rm H}$–variability can be stated, upper limits are shown. The distribution plotted as a histogram is found in Fig. 5. Both plots, Fig. 4 and Fig. 5, reveal a strong concentration towards shorter timescales from a few up to 10^3 days. One has to keep in mind that these plots may rather represent the situation of observation timing than a real source intrinsic distribution of variability timescales. The results of interest are the shortest timescales of each source, as listed in Table 2. Here we list only sources with sufficient data to constrain variability.

Source name	$\Delta t_{\min}$
NGC 3227	710 d
NGC 4593	2245 d
Mrk 704	235 d
Fairall 51	5 d
ESO 323-G077	455 d
Mrk 766	10 – 20 h [21]

TABLE 2. List of minimum timescales for all sources with sufficient data to constrain such timescales.

4. INTERPRETATION

The shortest variability timescales found are of particular interest, since they trace the smallest spatial scales of the absorber. To get an estimate on the distance of the variable absorber we assume distinct clouds to move across the line-of-sight on Keplerian orbits. A certain minimum cloud size is required to be able to cover the X-ray source and to derive upper limits on the distance of the absorber [20]. If the radius of the clouds moving on Keplerian orbits with velocity v around the central black hole is $r = xr_S$ where $r_S = 2GM/c^2$ is the Schwarzschild radius, and the time for the cloud to pass the line of sight is

$$\Delta t \sim 2r/v = 2xX^{1/2}r_S/c \tag{4}$$

with the distance of the absorber $R = Xr_S$ [10]. As X-ray sources of AGN are assumed to have a diameter of $10r_S$, the cloud diameter must be $> 10r_S$ in order to cover the central source [10]. The shortest measured timescale of 5 days is due to warm absorber variability. Together with a typical black hole mass of $10^8\,M_\odot$ [16] we find an absorber distance of $R \lesssim 1.42{\cdot}10^{16}$ cm. This distance is consistent with the distance to the BLR, which is around 0.001–0.1 pc, i.e., $3 \cdot 10^{15}$–$3 \cdot 10^{17}$ cm away from the black hole [3, 17, 19]. The result also fits well to the model of the BLR to consist of variable, ionized gas [3, 9]. The second minimal timescale found for one source is 235 d in the case of Mrk 704 (see Table 2). The according upper limit for the absorber distance estimated to be $R \lesssim 1.1 \cdot 10^{19}$ cm is consistent with the expected distance of the torus of a few parsec [8, 18].

ACKNOWLEDGEMENTS

This work has been funded by the Bundesministerium für Wirtschaft und Technologie under a grant from the Deutsches Zentrum für Luft- und Raumfahrt.

REFERENCES

[1] R. Antonucci, 2012, *Astronomical and Astrophysical Transactions*, 27, 557

[2] Barlow, R. 2004, arXiv:physics/0406120

[3] A. J. Blustin, et al., 2005, *A&A*, 431, 111

[4] S. Chakravorty, et al., 2008, *MNRAS*, 384, L24, doi:10.1111/j.1745-3933.2007.00414.x

[5] E. Costantini, 2010, *Space Sci Rev*, 157, 265, doi:10.1007/s11214-010-9706-3

[6] Dorodnitsyn, A., & Kallman, T. 2012, *ApJ*, 761, 70, doi:10.1088/0004-637X/761/1/70

[7] Fukumura, K., Kazanas, D., Contopoulos, I., & Behar, E. 2010, *ApJ*, 715, 636, doi:10.1088/0004-637X/715/1/636

[8] J. H. Krolik, et al., 1988, *ApJ*, 329, 702, doi:10.1086/166414

[9] J. H. Krolik, et al., 2001, *ApJ*, 561, 684, doi:10.1086/323442

[10] A. M. Lohfink, et al., 2012, *ApJ, Lett*, 749, L31, doi:10.1088/2041-8205/749/2/L31

[11] G. Matt, et al., 2011, *A&A*, 533, A1, doi:10.1051/0004-6361/201116443

[12] L. Miller, et al., 2007, *A&A*, 463, 131, doi:10.1051/0004-6361:20066548

[13] Markowitz, A. G., Krumpe, M., & Nikutta, R. 2014, *MNRAS*, 439, 1403, doi:10.1093/mnras/stt2492

[14] Nenkova, M., Sirocky, M. M., Ivezić, Ž., & Elitzur, M. 2008, *ApJ*, 685, 147, doi:10.1086/590482

[15] Nenkova, M., Sirocky, M. M., Nikutta, R., Ivezić, Ž., & Elitzur, M. 2008, *ApJ*, 685, 160, doi:10.1086/590483

[16] P. Padovani, et al., 1988, *A&A*, 205, 53

[17] B. M. Peterson., 1993, *PASP*, 105, 247, doi:10.1086/133140

[18] E. A. Pier, et al., 1992, *ApJ*, 401, 99, doi:10.1086/172042

[19] Reynolds, C. S., & Fabian, A. C. 1995, *MNRAS*, 273, 1167

[20] G. Risaliti, et al., 2002, *ApJ*, 571, 234, doi:10.1086/324146

[21] G. Risaliti, et al., 2011, *MNRAS*, 410, 1027, doi:10.1111/j.1365-2966.2010.17503.x

[22] J. E. Smith, et al., 2004, *MNRAS*, 350, 140, doi:10.1111/j.1365-2966.2004.07610.x

[23] T. J. Turner, et al., 2007, *A&A*, 475, 121, doi:10.1051/0004-6361:20077947